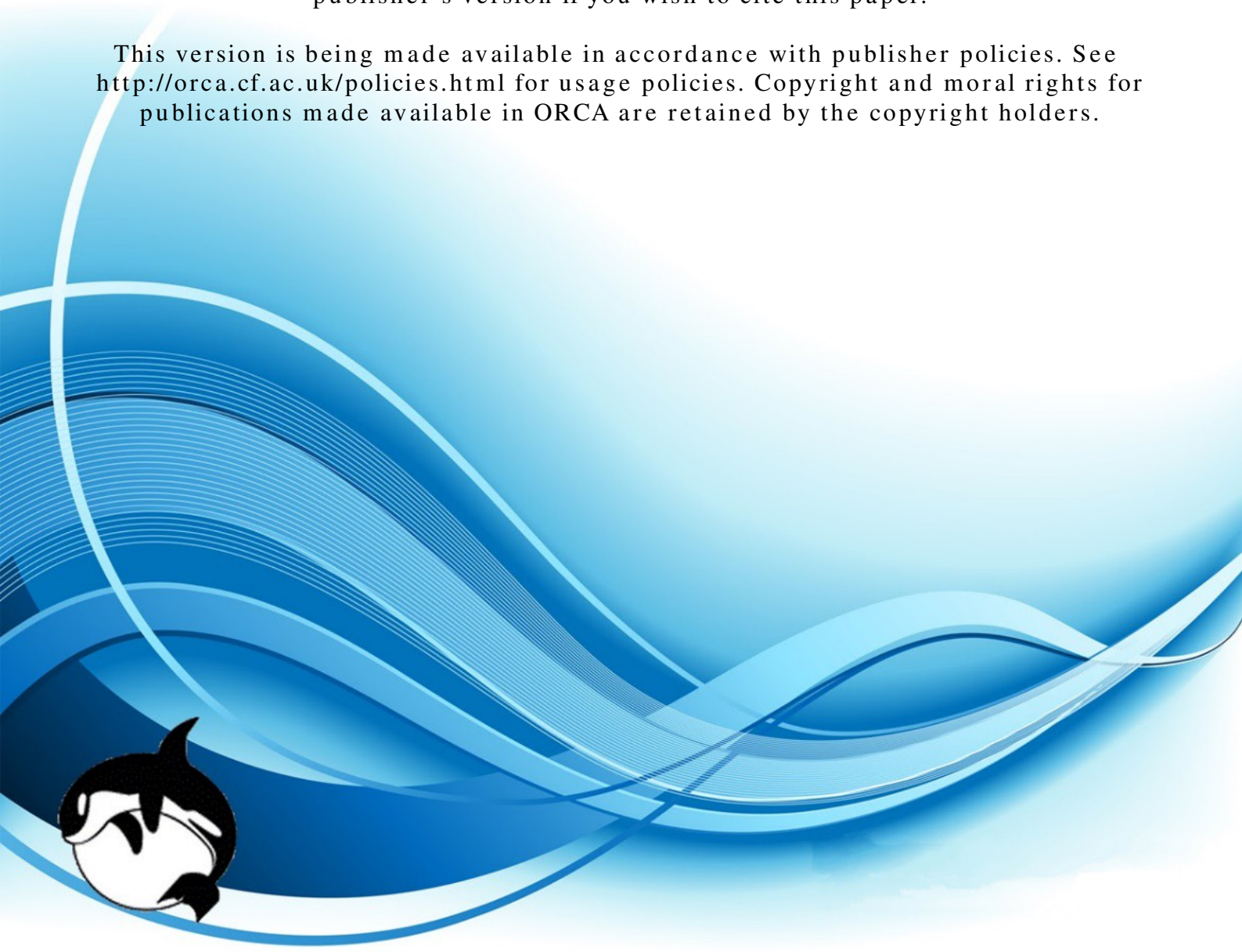

A comparison study of water diffusion in unidirectional and 2D woven carbon/epoxy composites

Faisel Almudaihesh, Karen Holford, Rhys Pullin, Mark Eaton.

Key words: Water absorption, Fibre architecture, Water ingress mechanism, Interfacial condition, and Moisture diffusion.

Abstract

The use of CFRP composites is significantly increasing in the aerospace, automotive and marine industries, particularly in safety critical primary structures. This work presents a newly developed experimental approach to investigate the directional diffusion of water in CFRP composites with the use of Fick's law. The approach is used to study the effect of fibre architecture on directional diffusion rates, with a particular focus on the role of fibre waviness in the diffusion process. A comparison of water diffusion is made in three different fibre architectures: unidirectional (UD), plain weave, and twill weave. The specimens were fully immersed in 90°C purified water until their maximum moisture saturation was achieved, with some specimens being selectively exposed from the edges only to obtain the directional diffusion coefficients. The water penetration process into the CFRP structure initiate from the micro-cracks and defects. The experimental work of this study shows sharp mass increases within the first stage followed by an equilibrium stage where saturation is present. The interfacial region is found to be a critical parameter where detachment of the interfacial fibre/matrix bonding is observed further demonstrating the potential effect of different fibre architecture in this region. UD fibre architecture showed ~20% higher diffusion coefficient in the $D_{x,y}$ direction compared

with plain and twill woven architectures. The weave patterns in 2D woven fibre architectures are therefore believed to play a key role on the moisture ingress mechanism and subsequently contributed in slowing down the capillary process in the interfacial region. This has implications for materials development and selection for CFRP composites used in moist environments.

1. Introduction

The influence of hygrothermal aging is a key factor that affects the mechanical performance of CFRP composites. It is of particular interest for structures operating in moist conditions, such as in the tidal energy sector where CFRPs are potential replacements for Glass Fibre Reinforced Plastics (GFRP) due to their very high specific mechanical properties [1]. Another attractive feature of CFRP is its high resistance to corrosion; elements such as chloride that exist in harsh marine environments can promote degradation of glass fibres. Gu reported that glass fibres lose 8% of their tensile strength when exposed to 2 wt% NaCI solution after one week of exposure [2]. Therefore carbon fibres are favoured over glass fibres [1, 3, 4] in the tidal energy sector. Whilst carbon fibres themselves are not susceptible to degradation from moisture exposure, the polymer matrix surrounding them is, due to hydrolysis which has a plasticizing effect leading to a reduction in properties [5–13]. This has led researchers to consider the consequential reduction of the matrix dominated properties in CFRP composites due to moisture absorption [5, 9, 14–18]. A loss of matrix dominated properties is seen by researchers with 26% reduction in short beam shear strength [7],

15% reduction in mode II fracture toughness [8], and a variety of 10%-50% reductions in compressive strength in stitched and unstitched unidirectional CFRP [19]. The incurred degradation in polymers due to hygrothermal aging has been shown to strongly depend on the constituent materials involved as well as the exposure environments [20–22]. Generally, moisture can diffuse easily and rapidly into polymers in the early stages, followed by a slow, gradual increase in the second stage, until equilibrium is reached and the material is saturated. This equilibrium stage is influenced by the geometry of the materials, where longer periods of months or even years are expected in larger structures prior to saturation [23, 24]. In the case of fibre reinforced polymers, debonding also occurs along the fibre/matrix interface [25–28], this behaviour is also seen in the authors previous work [29], giving rise to capillary transport. This accelerates moisture uptake into the composite, increasing the sorption rate of water into the polymer matrix which is directly related to the degradation of a polymer [30]. It is therefore believed that the fibre architecture is an essential parameter influencing the moisture penetration mechanism in composites. Increasing weave distortion leads to a more 'tortuous path' along the fibre matrix interface and therefore should yield lower diffusion coefficients. However, diffusion studies found investigated in literature along with their (experimental/modelling) approach and assumptions are mainly based on unidirectional fibre architectures [9, 21, 23, 31–35]. Therefore, this paper investigates the role of fibre architecture in the moisture diffusion process in CFRP composites. A new experimental approach is developed which enables the use of Fick's law to compare the directional diffusion coefficients of unidirectional and 2D woven CFRP composites.

2. Moisture Diffusion in Fibre Reinforced Composites

Fick's theory is frequently reported in modelling the moisture uptake process due to its suitability in determining moisture diffusion coefficients [24, 36] as compared with other theoretical approaches [36–38]. Bulk diffusion, D, from Fick's second law of diffusion, as postulated for composite materials, and the theoretical change in mass, M, of composite materials from water immersion, are given in Equation (1) and (2), respectively [39, 40].

$$D = \pi \left(\frac{h}{4M_\infty}\right)^2 \left(\frac{M_2 - M_1}{\sqrt{t_2} - \sqrt{t_1}}\right)^2 \left(1 + \frac{h}{L} + \frac{h}{w}\right)^{-2} \quad (1)$$

$$M = \left[1 - \frac{8}{\pi^2} exp\left(-\pi^2 \frac{Dt}{h^2}\right)\right] M_\infty \quad (2)$$

M_1 and M_2 are the moisture contents at times t_1 and t_2, respectively (observed from moisture uptake curve as illustrated in Figure 1); h is the distance into thickness; L is the composite length; w is the composite width; t is time; and M_∞ is the maximum change in mass.

Several fundamental parameters affect the diffusion coefficient in polymeric composites. The most notable being mainly attributed to temperature, where a small change in the temperature can cause a large change in the rate of diffusion [36]. Other factors include the chemical structure of the polymer, including the imperfections such as microcracks, and the degree of cross-linking [39]. The diffusion coefficient also depends on internal structure of CFRP composites such as the interphase region at the matrix/fibre interface where the polymer chains are pinned [41, 42]. Further complications also exist, such as the type of fibre sizing, the fibre surface roughness, the

microstructure of constituent contents, and the presence of structural defects [1, 41, 42].

Arnold *et al.* [31] carried out a study to determine the directional moisture diffusion coefficient of UD CFRP under 23°C, 40°C, and 70°C water immersion by using full 3D Fickian solution. Diffusivity across the fibres (y) and through the thickness (z) were 40%, and 13% of that found along the fibres (x), (as illustrated in Figure 2). The study also compared diffusion in unreinforced resin with 'along the fibre' diffusion and the results showed slightly lower diffusion rates for the unreinforced resin, indicating an effect from the interface and interphase regions between the fibre and matrix [31]. Similarly Zafar et al. [9] investigated the long-term effects of moisture on pure epoxy and CFRP composites in seawater and demineralised water at ambient temperature for up to 300 days. The pure epoxy specimens initially gained mass linearly and reached saturation at moisture contents of 1.79% and 2.03% for seawater and demineralised water, respectively, after 40 days. The composite specimens exhibited a more rapid linear increase compared with the pure epoxy specimens and reached saturation at moisture contents of 2.18% and 2.31%, for the seawater and demineralised water, respectively, after 57 days. The bulk diffusion coefficients ($x10^{-14}$ m^2/s) were found to be 7.89 and 8.4 for pure epoxy in seawater and demineralised water, respectively and 11.9 and 12.6 for composite specimens in seawater and demineralised water, respectively. The authors believe that the equilibrium moisture content and diffusion coefficient values for composites specimens were higher due to the imperfect interface between the fibre and matrix. Therefore, the moisture transport in the composite specimens is also governed by capillary transport into the gaps at the interfacial regions [9]. The study suggested

that the observed higher moisture contents found in those specimens exposed to demineralised water, compared with their equivalents in seawater, was due to the presence of salt in the seawater, which reduces the activity of the water molecules because salt particles are less readily absorbed [9]. The accumulation of salt particles on the surface of the specimens could inhibit the water absorption, the concentration of salt particles in the seawater inside the epoxy specimen is less than that in the surrounding seawater, which would result in a creation of an osmotic pressure that acts against the water absorption [9]. Therefore, the equilibrium moisture is lower for the specimens in the seawater as compared with the specimens in demineralised water [9].

Grammatikos *et al.* [24] studied the directional diffusion coefficients for pultruded fibre reinforced polymers (PFRP) at 60°C. To achieve this, specimens were prepared in a way that exposed an opposing pair of edge surfaces that are perpendicular to the direction of moisture uptake being characterised [24]. A <1 mm epoxy layer and an aluminium tape layer of ≈30μm thickness were applied to the four non-exposed surfaces to act as a barrier to moisture. The results of this study with the use of equation (2), and without taking into account the last dimensional parameter to correct for the edge effects which showed directional diffusion coefficients ($x10^{-6}$ mm^2/s) for the PFRP 6.4 mm flat sheet of 9.26, 7.04, and 1.85 for D_x, D_y, and D_z, respectively [24]. Another calculation approach was also employed in the same study with the use of 3D diffusion approximation originally reported by Shen *et al.* [40] where from the linear part of the moisture sorption curve one can approximate a three dimensional behaviour by using Equation (3).

$$D = D_z \left(\frac{h}{l} \sqrt{\frac{D_y}{D_z}} + \frac{h}{w} \sqrt{\frac{D_x}{D_z}} + 1 \right)^2 \quad (3)$$

Where D in this equation is the bulk moisture diffusion, h in the thickness of the specimen, l is the length, and d is the width, x, y, and z are the directional configuration (Figure 2). In order to determine the directional diffusion coefficients with the use of equation (3). The study used the same water exposure conditions but with specimens with different aspect ratios to determine directional diffusion coefficients (x 10^{-6} mm^2/s) of 44.8, 5.26, and 0.55 for D_x, D_y, and D_z, respectively. The study concluded that the differences in directional D values observed from the two different approaches can be attributed to the differences in test methodology in terms of specimens geometry, as well as the assumptions involved in the mathematical and experimental approximation employed for their determination [24].

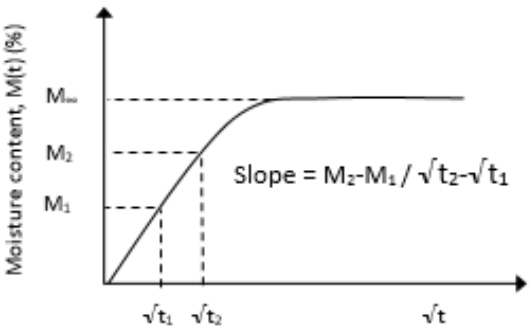

Figure 1: Representative of classical Fickian diffusion three-stage curve for M(t) vs. √t.

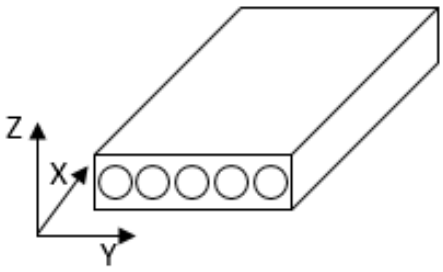

Figure 2: Directional configuration.

From literature, the directional diffusions are observed by selectively blocking the water uptake from certain directions of the specimens and applying equation (1) or exposing specimens with three different geometrical aspect ratios and applying equation (3). Both approaches require a number of assumptions in the experimental approach and therefore lead to significant variations in the reported results. For example, in Grammatikos's *et al.* [24] study where the authors introduced an epoxy layer and aluminium tape to the four non-exposed surfaces to act as a barrier to moisture uptake, significant changes in the directional diffusion results were observed for the same materials compared with when applying the geometrical aspect approach. The authors correlated these differences to the test methodology, as well as the assumptions involved in the mathematical approximation employed, further demonstrating the rule on the use of different experimental approach [24]. In ASTM D5229 [43], it states that in the case where a mask/barrier is used then it should be ensured that materials used have no influence on the mass gain of the sample. This is important as the mass gains measured during diffusion studies are very small and even very small errors in mass change can lead to significant uncertainty in the calculated diffusion coefficients. It is not made clear in most published studies what influence the barrier configuration has and it adds significant experimental cost to carefully determine the influence of any coating. For the second approach, three different geometrical aspect ratios of specimens are needed to determine the directional diffusion for each fibre architecture. Therefore, the number of specimens is significantly increased and additionally the influence of short edges is deemed to be negligible, however these will still have an influence on the total mass gain. Therefore, in this work, the novelty derives from the

experimental approach developed which helps to minimise the assumptions made experimentally and exclude any physical attachment of barriers that could lead to confusions in the results between the different directional diffusion rates in different fibre architectures.

3. Experimental Methods

3.1 Materials

In this work, three versions of CFRP prepreg with different fibre architectures were used. The fibre architectures used were selected due to their current high consumptions across different industries [44]. All were manufactured by SK Chemicals using Skyflex K51 Epoxy resin in order to eliminate the influence of polymer type. The specification of each prepreg variant used were: 15k UD, Pyrofil TR50S high strength carbon fibre 200gsm with 33% resin content (V_m); 3k plain weave, Pyrofil TR30S high strength carbon fibre 198gsm with 40% resin content; and 3k 2x2 twill weave, Pyrofil TR30S high strength carbon fibre 198gsm with 40% resin content. Fibres sizing levels were 1.0% and 1.2% for Pyrofil TR50S and Pyrofil TR30S, respectively. All carbon fibres featured the same filament diameter of 7um. All materials were cured with the same cure cycle, as recommended by the material supplier, using an autoclave under two dwells: 30 minutes at 80°C temperature and 5 bar pressure followed by 60 minutes at 125°C temperature and 5 bar pressure. Sixteen ply panels with stacking sequences of $[0/90]_8$ (for UD) and $[(0/90)]_{16}$ (for woven) were manufactured producing thicknesses of 3.07mm, 3.54mm, and 3.51mm for UD, plain, and twill, respectively. The panels were then cut into 40mm (±0.3mm) long by 40mm width (±0.3mm) specimens with a diamond

blade (using Acmitaly cutting machine, model ACM BS 740). The stacking sequences applied enabled an identical distribution of fibre directions between the UD and woven specimens for comparison purposes. This also allows the assumption that diffusion along the fibre (x-axis) is equal to the diffusion across the fibres (y-axis) in both UD and woven specimens (hence, the square shape for the specimens was desired). To enhance tolerances and edge finishes, a rotor polishing machine by Struers model Knuth-Rotor-3 with silicon carbide grinding paper grit 320 was used. All specimens were C-scanned to ensure manufacturing quality.

3.2 Moisture Conditioning

The aging procedures applied for the moisture conditioning were in accordance with ASTM D5229 [43]; however, a higher water temperature (90°C versus the 70°C recommended) was chosen to accelerate the ageing process and monitor the mass change. In order to obtain a realistic prediction of long-term moisture behaviour, the temperature has to be lower than the polymers glass transition temperature (T_g), by 20°C according to Bank et al. [45]. For the E51 Epoxy resin used in this study the tg has been measured by Dynamic Mechanical Analysis (DMA), in accordance with ASTM D7028 [46], to be 122.83°C. This is to avoid the secondary degradation mechanism (excessive unwanted degradation) which activates when the temperature is near or exceeds the T_g and does not replicate the ambient temperature diffusion scenario [20, 47]. The water absorption testing was carried out by a gravimetric method. This was achieved by using non-ambient moisture conditioning in a water immersion tank at 90°C for 100 days. Purified water (type 1) was used and an unstirred digital bath (NE2-28D)

supplied by Clifton was used. The tank has a sensitivity of ±0.2°C and uniformity of ±0.1°C with a stainless steel hinged gable lid (to reduce water evaporation). The specimens were placed in the water bath, which had previously reached the specified steady-state temperature. For weighing records, specimens were individually removed from the water bath (and unmasked for the selectively exposed specimens) and left in a sealed bag until they reached an acceptable temperature for laboratory handling (room temperature). Samples were then removed from the bag and wiped using absorbent cloth, before measuring their mass change using an analytical balance with accuracy of 0.0001g (Sartorius LA310S analytical balance). the samples were then returned to the water bath (after remasking the selectively exposed specimens). The specimen water content was determined as a percentage change using Equation (4):

$$Mass\ percentage\ change, \% = \left(\frac{W_i - W_o}{W_o}\right) \times 100 \qquad (4)$$

W_i is weight of the specimen at each point of the weight recorded during the experiment and W_o = initial dry weight of the specimen before any contact with water.

All specimens were dried for 24 hours at 30°C in an oven prior to water immersion to make sure they are free from moisture that could be caused by the manufacturing process or prior storage

3.3 Diffusion Calculations

The diffusion coefficients in this work were obtained by employing Fickian theory with the assumption of uniform moisture and temperature conditions throughout the

volume using Equation (1), which was initially developed from Fick's transient equation (Equation (5)) by Crank [39].

$$\frac{\partial z}{\partial t} = D\frac{\partial^2 C}{\partial z^2} \quad (5)$$

Z is the distance into the thickness (h) from an exposed surface, and C is the concentration of water.

The experimental approach used in this study included a physical isolation of the two surfaces of each specimen (top and bottom flat surfaces) to stop moisture from penetrating in the (Z-axis). When immersed in water only the four side edges only for each fibre architecture (five specimens for each fibre architecture) to calculate the $D_{x,y}$ (D_x and D_y are assumed to have equal values due to same distribution of fibre directionality in all edges). In addition, another five specimens for each fibre architecture were fully exposed in order to obtain the maximum saturation. Figure 3 presents the set up for the fixture used to eliminate the water exposure from the (z-axis) direction, whereas Figure 4 presents the schematic detailing assembly. A neoprene rubber (chloroprene/SBR CQ grade) was added between the toughened glass and the CFRP specimens which is generally used for the purpose of gasket and engineering applications, therefore very resistant to mineral oil, gases, water, UV, ozone, mild chemical, acids. It was essential to add the neoprene rubber to the assembly so the surfaces of the CFRP specimens are submerged into the rubber when the outer toughened glass layers are clamped (at corners and edges of glass) as highlighted in Figure 4. Thus eliminating the penetration of water from the edges to the surface,

allowing the assumption that the z-axes of the specimens have absorbed negligible amount of water.

In summary, the selectively exposed specimens were used to obtain (M_1 at $\sqrt{t_1}$, and M_2 at $\sqrt{t_2}$ from Figure 1) in order to calculate $D_{x,y}$. The fully exposed specimens were used to obtain M_∞ to reach saturation (maximum moisture content) since both the selectively and fully exposed specimens are the same materials and are expected to have the same maximum moisture content. This enables the use of equation (1) excluding the last dimensional factor due to specimens being selectively exposed and assuming Fickian behaviour is present. 96 hours of water immersion for the selectively exposed specimens are believed to be enough to obtain the curve from which the (M_1 at $\sqrt{t_1}$, and M_2 at $\sqrt{t_2}$) values are attained. This duration was also limited by the peel up of the surfaces in contact with the rubber when disassembling the clamps for measurements after longer durations.

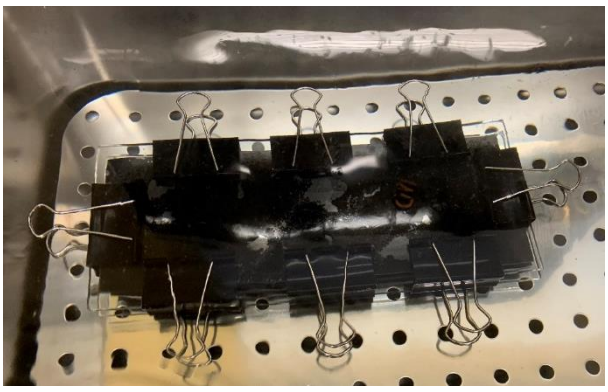

Figure 3: Water diffusion fixture assembly set up.

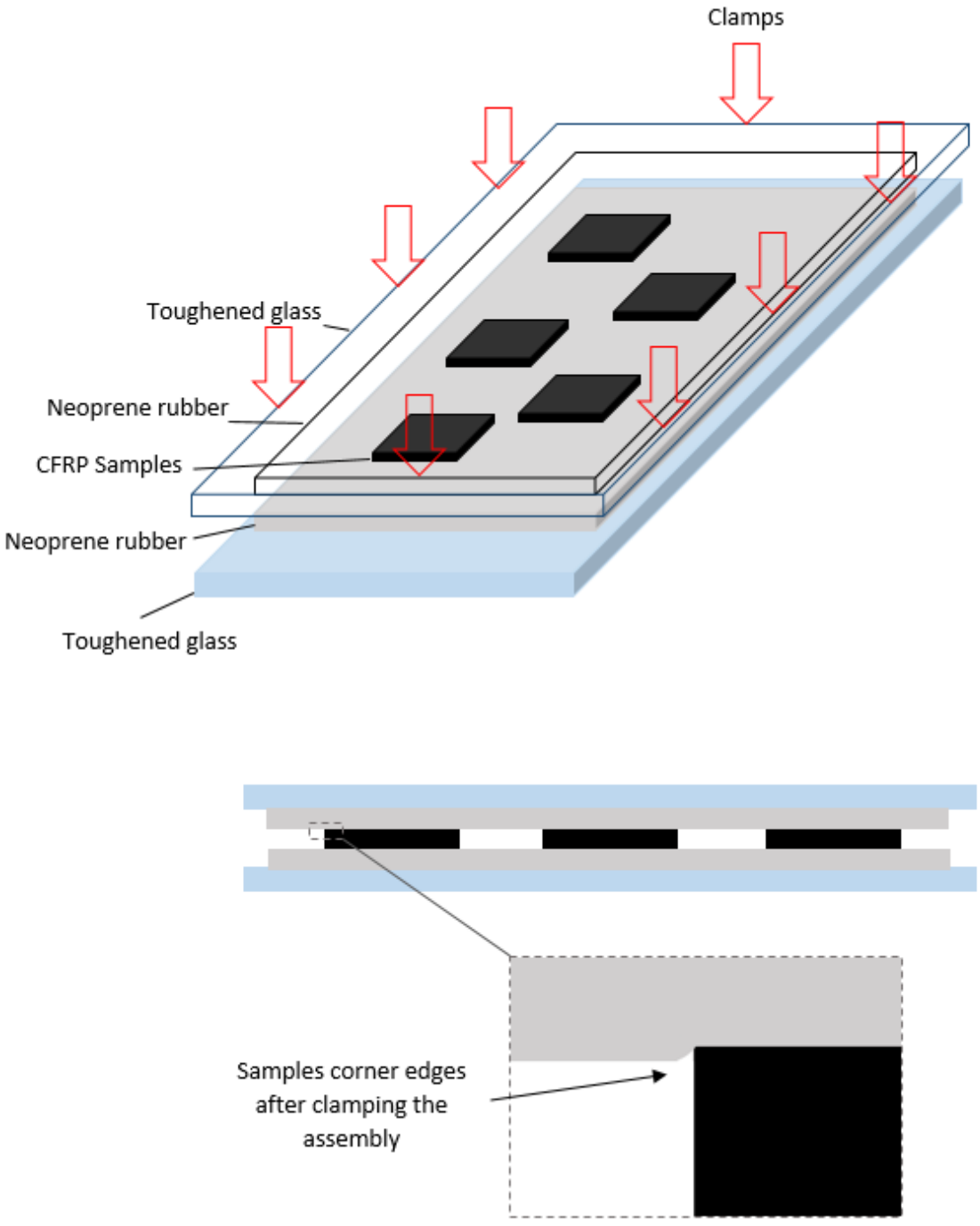

Figure 4: Schematic detailed assembly for water diffusion fixture.

4. Results and Discussion

Figure 5 presents the average mass change for UD, plain, and twill weave CFRP composites following water exposure for 100 days and subsequent oven drying for 15 days (errors bars represent the standard deviation). It shows that the moisture uptake process follows a classical Fickian trend. The moisture uptake curves (Figure 5) illustrate a gradual moisture uptake at the initial stage until an equilibrium stage (saturation) is reached. The mass change curves then fluctuate with very minimal mass changes (upwards and downwards), suggesting one of two potential mechanisms. The first is the potential occurrence of degradation mechanisms taking place whilst moisture uptake continues within the structure, which has been shown to leading to fluctuation in mass changes [24, 48]. The second potential cause is the scatter within the mass measurements [43] (with the mass change values being very small at this stage).

The UD specimens reached a maximum value of mass change after 31 days of water immersion at 90°C. The Plain and twill weave specimens reached their maximum values of mass change after 45, and 43 days of water immersion, respectively (Table 1). It is expected that the woven specimens would take a longer time to reach maximum mass change due to higher V_m. However, given the fluctuation in mass observed in the 'plateau' region (Figure 5), taking the absolute maximum value of mass gain achieved as the point of saturation is somewhat arbitrary. Instead, the point of saturation has been taken as the point at which the rate of daily mass change becomes less than 1% of the total mass gain (taken as the absolute maximum recorded). Figure 6 presents the daily mass change as a percentage of total observed mass gain. In the case where sequential

gravimetric measurements are taken more than one day apart, the percentage change is divided by the number of days between measurements (to give a daily rate). This shows that UD and twill weave specimens reached saturation after 16 days, whereas the plain weave specimens reached saturation after 20 days. However, no gravimetric measurements were collected between 17-20 days, so it is possible that saturation of the plain weave sample could have occurred at an earlier point between 17-20 days.

Following oven drying for 15 days the sample masses were seen to be below that of the original specimens (Figure 5). This demonstrates that the specimens had reached their maximum moisture uptake (saturation) and were subsequently subject to degradation of the matrix [24].

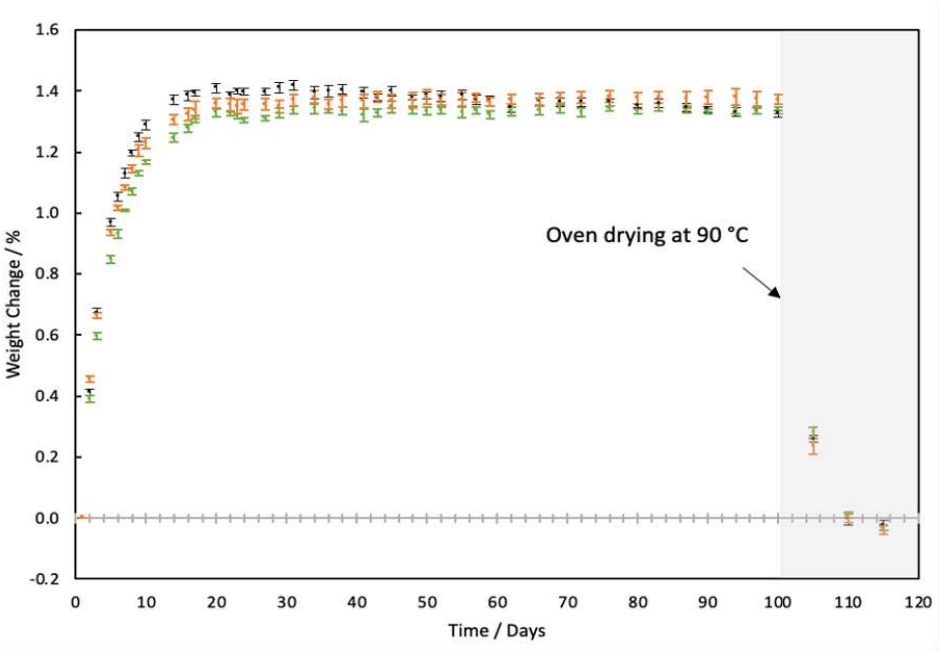

Figure 5: Water uptake for water diffusion experiment.

Table 1

Mass change data observed for all fully exposed specimens.

Day (hours)	Mass Change (%)			Day (hours)	Mass Change (%)		
	UD	Plain	Twill		UD	Plain	Twill
1 (0)	0.000	0.000	0.000	43 (1008)	1.379	1.327	1.381
2 (24)	0.412	0.390	0.456	45 (1056)	1.400	1.348	1.366
3 (48)	0.672	0.595	0.664	48 (1128)	1.379	1.337	1.369
5 (96)	0.969	0.848	0.936	50 (1176)	1.384	1.335	1.381
6 (120)	1.054	0.931	1.017	52 (1224)	1.381	1.337	1.372
7 (144)	1.129	1.009	1.083	55 (1296)	1.387	1.330	1.371
8 (168)	1.197	1.070	1.144	57 (1344)	1.371	1.337	1.377
9 (192)	1.250	1.132	1.205	59 (1392)	1.368	1.323	1.364
10 (216)	1.289	1.167	1.229	62 (1464)	1.345	1.332	1.372
14 (312)	1.371	1.247	1.306	66 (1560)	1.366	1.337	1.371
16 (360)	1.384	1.278	1.322	69 (1632)	1.363	1.342	1.376
17 (384)	1.392	1.309	1.337	72 (1704)	1.363	1.330	1.379
20 (456)	1.410	1.330	1.359	76 (1800)	1.363	1.342	1.381
22 (504)	1.386	1.325	1.354	80 (1896)	1.352	1.332	1.376
23 (528)	1.400	1.318	1.349	83 (1968)	1.360	1.346	1.379
24 (552)	1.397	1.304	1.354	87 (2064)	1.345	1.337	1.374
27 (624)	1.397	1.311	1.357	90 (2136)	1.339	1.332	1.379
29 (672)	1.410	1.327	1.349	94 (2232)	1.331	1.339	1.381
31 (720)	1.418	1.337	1.369	97 (2304)	1.334	1.335	1.374
34 (792)	1.394	1.342	1.379	100 (2376)	1.326	1.337	1.372
36 (840)	1.400	1.335	1.357	105 'oven dried'	0.260	0.281	0.235
38 (888)	1.405	1.334	1.367	110 'oven dried'	-0.003	0.009	0.000
41 (960)	1.394	1.320	1.366	115 'oven dried'	-0.024	-0.033	-0.037

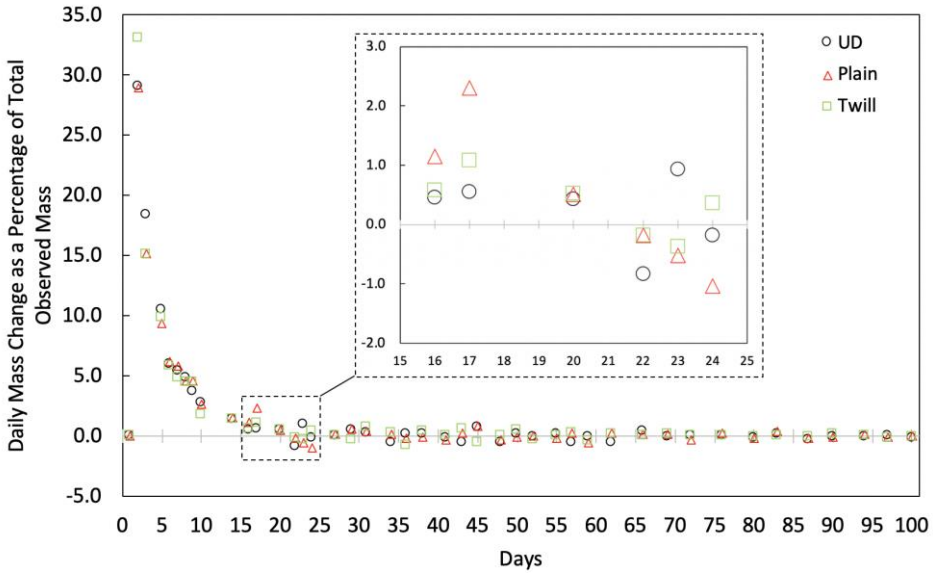

Figure 6: The rate of daily mass change as a percentage of total observed mass gain versus immersion time.

Table 2 presents the values of M1 and M2 recorded at time point $\sqrt{t_1}$ and $\sqrt{t_2}$, respectively, for the fully exposed and the edges exposed specimens.

Table 2

$\sqrt{t_1}$, $\sqrt{t_2}$, M1 at $\sqrt{t1}$ for fully exposed specimens and edges exposed specimens, and M2 at $\sqrt{t2}$ observed for fully exposed specimens and edges exposed specimens.

Fibre type	$\sqrt{t_1}$	$\sqrt{t_2}$	Fully Exposed M_1 at $\sqrt{t_1}$	Fully Exposed M_2 at $\sqrt{t_2}$	Edges Exposed M_1 at $\sqrt{t_1}$	Edges Exposed M_2 at $\sqrt{t_2}$
UD (cross-ply)	√24	√96	0.412	0.969	0.381	0.857
Plain	√24	√96	0.39	0.848	0.356	0.792
Twill	√24	√96	0.456	0.936	0.325	0.774

From the observed data in Table 1 and Table 2 $D_{x,y}$ can be calculated using equation (1) by excluding the last dimensional factor (due to specimens being selectively exposed). The calculation of D_z is then feasible by subtracting M_1 and M_2 observed for the edges exposed specimens from M_1 and M_2 observed for the fully exposed specimens. Figure 7 presents the average directional diffusion coefficients observed in this study (errors bars represent the standard deviation).

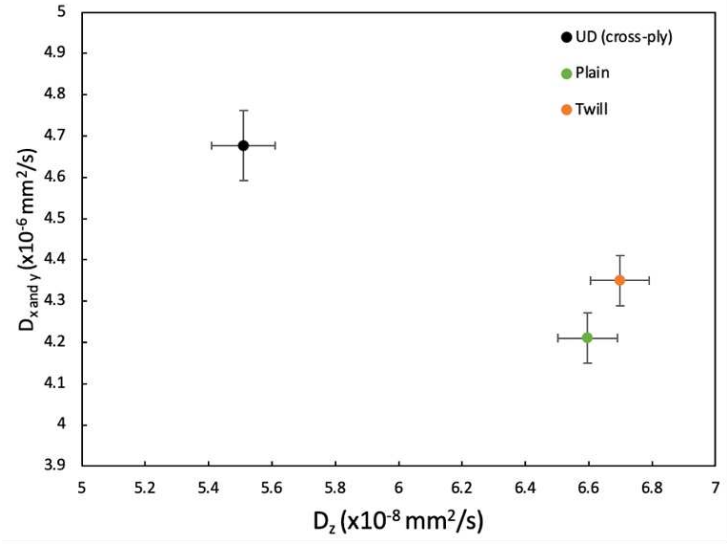

Figure 7: Water diffusion coefficients for UD, plain, and twill.

In general, and in line with the literature, the $D_{x,y}$ values are greater than the D_z values in all fibre architectures [24, 31]. This further demonstrates that the rise in moisture ingress along the fibres is mainly attributed to the raise in capillary process due fibre/matrix interface [9, 32], and the unidirectional nature the UD fibre architecture, further accelerated this process. Table 3 presents the data observed for directional diffusion rates from the literature and from this study. It is seen that there are significant variations in the D_z values across all studies, particularly when compared with the data of this paper. This can be correlated to the experimental approach used. It is worth noting that the specimens used in this study are to aerospace standards with less than 1% void content rate as reported in a previous study [29]. Given that the surface on the (D_z) direction had no manufacturing post-process cutting, unlike the ($D_{x,y}$) direction, this side is expected to have minimal moisture uptake, particularly with the purified water used in this study (which excluded the natural elements as this could accelerate the matrix aging process in introducing matrix cracking [7, 16]). Whereas the cutting process

applied to the ($D_{x,y}$) direction edges leads to surface damage that provides direct access to the fibre/matrix interface along with the matrix cracking which accelerates the moisture penetration process [29]. Given that the results were observed by an experimental approach that excluded any attachment of barrier materials, that could influence mass gain measurements, the authors are confident that these values provide a more accurate representation of the directional diffusion behaviour. Given the identical methodology used for each sample in this study and the confidence in the validity of the results, they can be used for comparison purposes between the different fibre architectures in the specimens tested. Table 3 also highlights how different approaches to calculating diffusion coefficients can result in very different reported results. Even when the same testing set-up is used to record data, the litrature show significant differences in the final values [24] which demonstrate that the assumptions made in each study can lead to significant changes in the final results.

Table 3

Directional Diffusion Results From literature and this Study.

	$D_{x,y}$	D_z	Percentage ratio of D_z to D_{xy} (%)
Arnold *et al.* [31] at 23°C Water	8.6 ($m^2/s \times 10^{14}$)	1.8 ($m^2/s \times 10^{14}$)	20.90
Arnold *et al.* [31] at 40°C Water	23.45 ($m^2/s \times 10^{14}$)	4.16 ($m^2/s \times 10^{14}$)	17.70
Arnold *et al.* [31] at 70°C Water	122.07 ($m^2/s \times 10^{14}$)	24.83 ($m^2/s \times 10^{14}$)	20.34
Grammatikos *et al.* [24] (Equation 2) at 60°C Water	8.15 ($mm^2/s \times 10^{-6}$)	1.85 ($mm^2/s \times 10^{-6}$)	22.70
Grammatikos *et al.* [24] (Equation 3) at 60°C Water	25.03 ($mm^2/s \times 10^{-6}$)	0.55 ($mm^2/s \times 10^{-6}$)	2.20
Huo *et al.* [35] at 50°C Water	1.45 ($mm^2/s \times 10^{-6}$)	0.37 ($mm^2/s \times 10^{-6}$)	25.52

Huo *et al.* [35] at 90°C Water	9.36 ($mm^2/s \times 10^{-6}$)	2.02 ($mm^2/s \times 10^{-6}$)	21.58
Results from this study for UD	4.67 ($mm^2/s \times 10^{-6}$)	0.055 ($mm^2/s \times 10^{-8}$)	0.012
Results from this study for Plain	4.18 ($mm^2/s \times 10^{-6}$)	0.065 ($mm^2/s \times 10^{-8}$)	0.016
Results from this study for Twill	4.35 ($mm^2/s \times 10^{-6}$)	0.066 ($mm^2/s \times 10^{-8}$)	0.015

The trend in the D values from this study suggests that the crimp pattern of the fibre weaves is playing an essential role in the differences observed. The UD showed 19.69% and 21.56% higher diffusion coefficients in the $D_{x,y}$ direction compared with plain and twill weaves, respectively. The trend in $D_{x,y}$ with fibre architecture supports the 'tortuous path' hypothesis, with greater fibre warping leading to lower diffusion rates. This corresponds to theoretical predictions made by Choi et al [49], who showed that as fibre angle increases relative to diffusion direction the diffusion coefficient decreases. Figure 8 illustrates the water paths in the three fibre architectures studied here. It shows how the amount of parallel fibres in the $D_{x,y}$ direction decreases from UD to Twill weave to Plain weave and corresponds to the change in diffusion coefficient measured.

The D_z direction is however lower in the UD by 9.98% and 7.01% as compared with plain and twill, respectively. As observed from the literature that the interfacial region is critical in the capillary process [50–52], it is believed that the D_z is higher in the woven samples than the UD sample due to the fact that the weave pattern of the fibres in one ply is allowing easier transfer of water to the neighbouring fibres (through the crimp) allowing a faster water diffusion per ply set in the D_z direction. Unlike the UD where each fibre bundles are uniformly separated by the matrix from the D_z direction.

To further investigate the role of the fibre matrix interface on the diffusion process SEM (captured using a ZEISS Sigma HD SEM) analysis of UD specimens was undertaken before and after aging. The SEM images are shown in Figure 9Figure 11 for dry and 43-day aged specimens. Clear evidence of degradation and debonding of the fibre matrix interface can be seen in the aged specimens, further demonstrating the role of the interfacial region in diffusion. This supports the hypothesis that fibre architecture plays an important role in the moisture penetration mechanism of CFRP materials. From these results it is clear that fibre architecture influences diffusion rates but further investigation using equivalent matrix volume fractions and fibre sizing levels would help to further isolate this effect and clarify its significance.

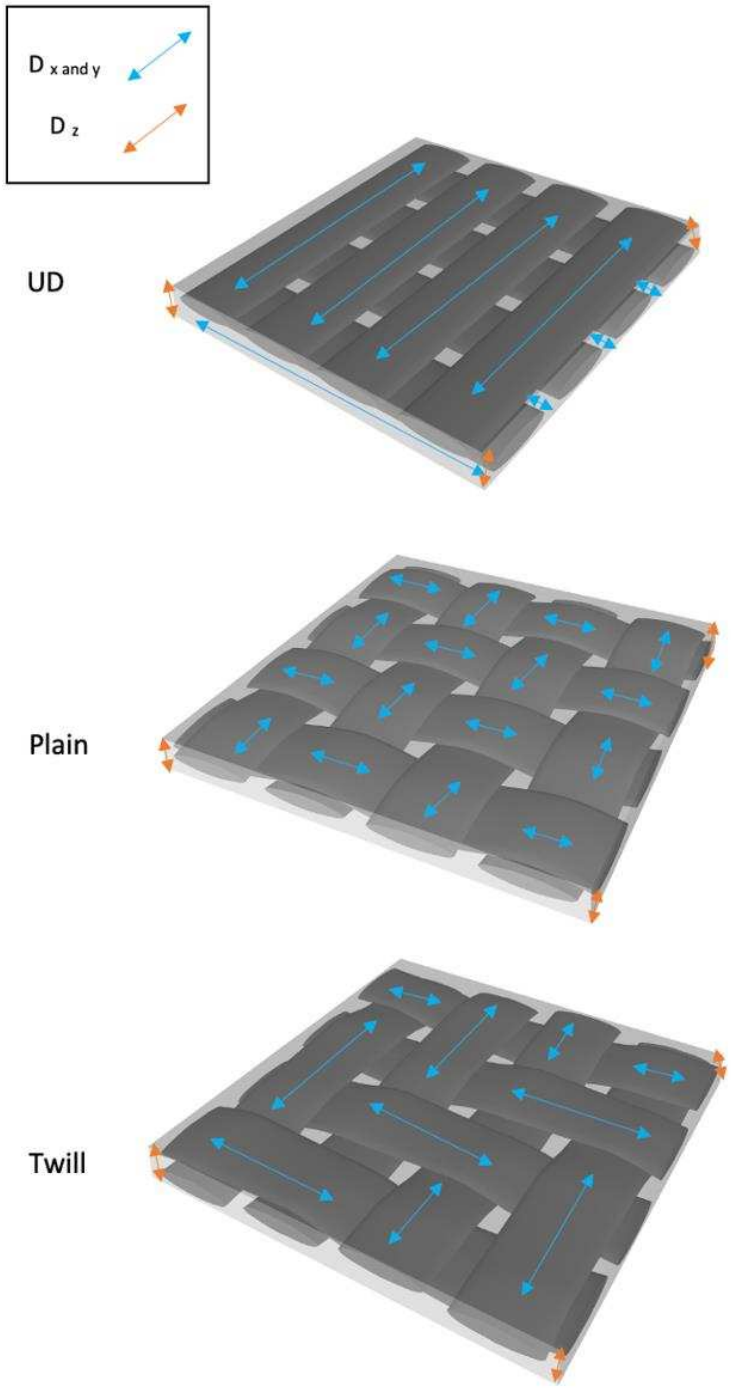

Figure 8: Penetraion paths in different fibre weaves.

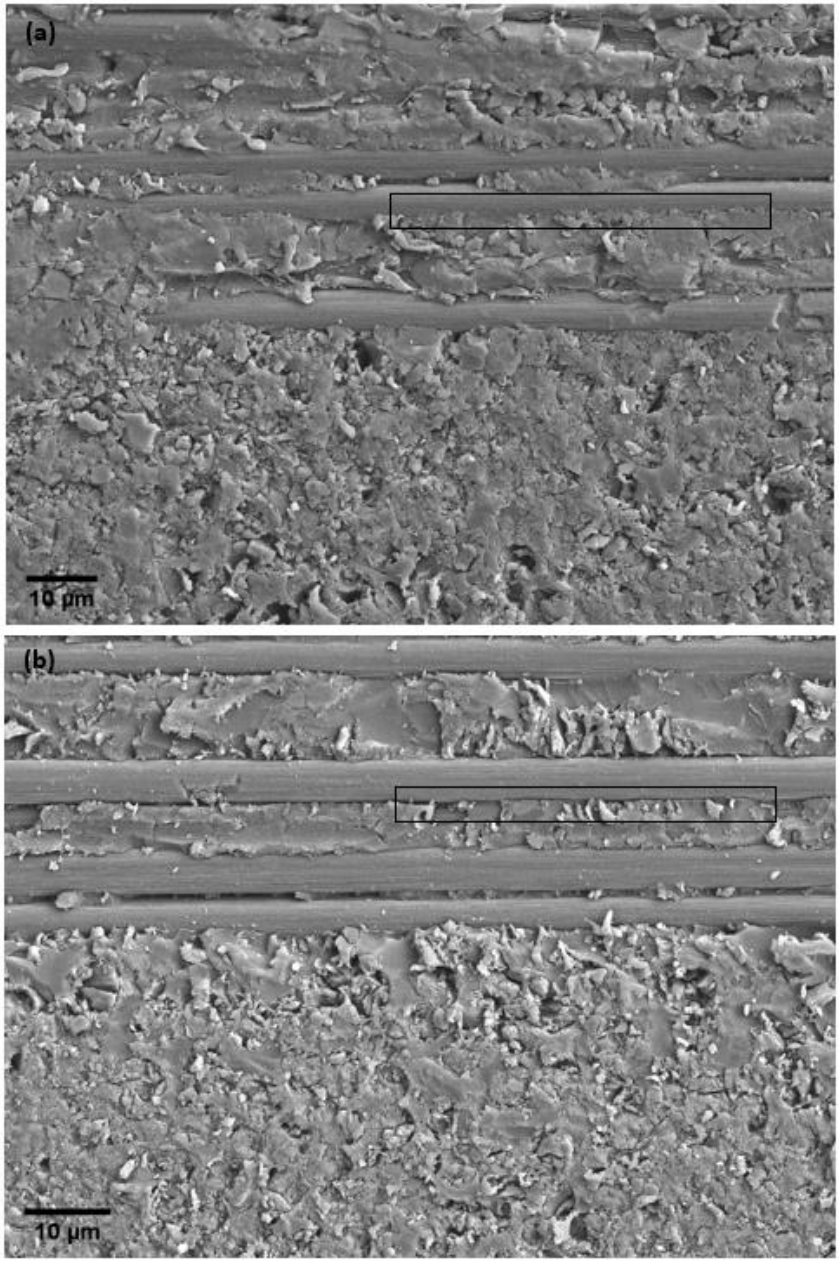

Figure 9: SEM comparison images of; (a) dry UD, (b) after 43 of water immersion in purified water at 90°C for a UD specimen.

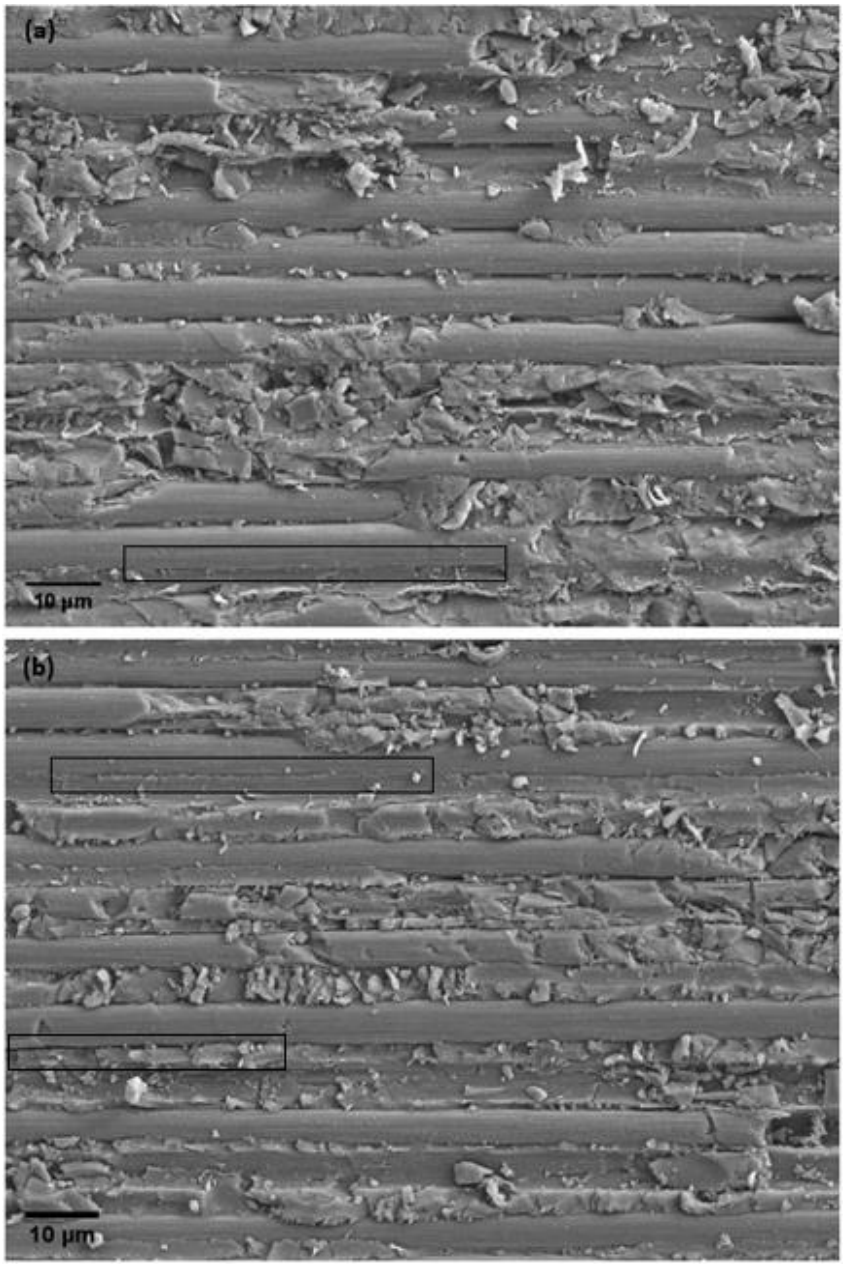

Figure 10: SEM comparison images of a 90° UD layer; (a) dry, (b) after 43 of water immersion in purified water at 90°C.

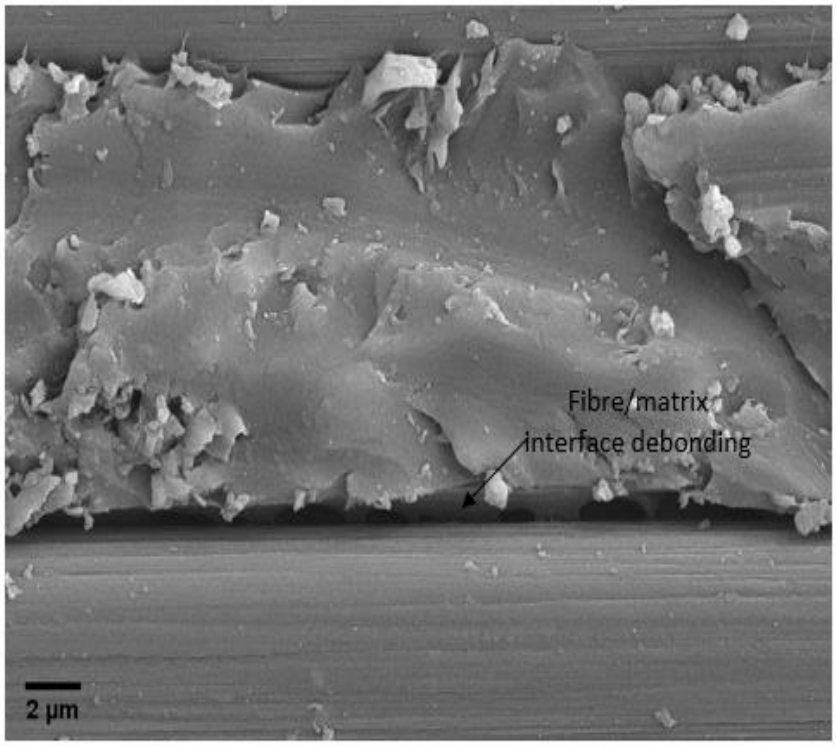

Figure 11: The interfacial condition in a UD specimen after 43 of water immersion in purified water at 90°C.

5. Conclusions

A new experimental method was developed to measure the diffusion coefficients from the edges ($D_{x,y}$) and through the thickness (D_z). This enabled a comparative study of the diffusion behaviour in UD and 2D Woven CFRP composites. A clear correlation between crimp pattern and diffusion rate was observed. Higher diffusion coefficients were observed for UD architecture compared with the woven architectures, where a more 'tortuous path' for capillary transport along the woven fibres slows the water penetration process. UD fibres showed 19.69% and 21.56% higher diffusion coefficients in the $D_{x,y}$ direction compared with plain and twill weaves, respectively. The through

thickness diffusion (D_z) was observed to be lower in the UD specimens by 9.98% and 7.01%, compared with plain and twill, respectively. This is believed to be due to the resin paths present between overlapping fibre tows and orientation of fibres towards the through thickness direction within the weave patterns.Even though the UD material featured slightly lower levels of sizing (1% versus 1.2%) and resin content (33% versus 40%) the observed trends are still clear in the woven materials, which had identical constituent properties. The differences in diffusion coefficients observed from the experimental approach applied in this study with the use Fick's law are large enough to suggest that the fibre architecture is having a significant influence on moisture penetration mechanisms (particularly considering that the lower matrix volume fraction in the UD material would likely lead to lower moisture uptake). This could prove to be important for mechanical property retention in moist environments and is a consideration when selecting materials for use in such environments.

6. References

[1] Alam P, Robert C, Ó Brádaigh CM. Tidal turbine blade composites - A review on the effects of hygrothermal aging on the properties of CFRP. *Compos Part B Eng* 2018; 149: 248–259.

[2] Gu H. Tensile behaviours of quartz, aramid and glass filaments after NaCl treatment. *Mater Des* 2009; 30: 867–870.

[3] Staudigel H, Chastain RA, Yayanos A, et al. Biologically mediated dissolution of glass. *Chem Geol* 1995; 126: 147–154.

[4] Wei B, Cao H, Song S. Degradation of basalt fibre and glass fibre/epoxy resin

composites in seawater. *Corros Sci* 2011; 53: 426–431.

[5] Pérez-Pacheco E, Cauich-Cupul JI, Valadez-González A, et al. Effect of moisture absorption on the mechanical behavior of carbon fiber/epoxy matrix composites. *J Mater Sci* 2013; 48: 1873–1882.

[6] Saito H, Kimpara I. Damage evolution behavior of CFRP laminates under post-impact fatigue with water absorption environment. *Compos Sci Technol* 2009; 69: 847–855.

[7] Kafodya I, Xian G, Li H. Durability study of pultruded CFRP plates immersed in water and seawater under sustained bending: Water uptake and effects on the mechanical properties. *Compos Part B Eng* 2015; 70: 138–148.

[8] Selzer R. Mechanical properties and failure behaviour of carbon fibre-reinforced polymer composites under the influence of moisture. 1997; 595–604.

[9] Zafar A, Bertocco F, Schjødt-Thomsen J, et al. Investigation of the long term effects of moisture on carbon fibre and epoxy matrix composites. *Compos Sci Technol* 2012; 72: 656–666.

[10] Li H, Zhang K, Fan X, et al. Effect of seawater ageing with different temperatures and concentrations on static/dynamic mechanical properties of carbon fiber reinforced polymer composites. *Compos Part B Eng* 2019; 173: 106910.

[11] Almudaihesh F, Grigg S, Holford K, et al. An Assessment of the Effect of Progressive Water Absorption on the Interlaminar Strength of Unidirectional Carbon/Epoxy Composites Using Acoustic Emission. *Sensors* 2021; 21: 4351.

[12] Attukur Nandagopal R, Narasimalu S, Chai GB. Study of statistically significant strength degradation of hygrothermal aged CFRP and its weibull analysis. *Compos Commun* 2021; 23: 100566.

[13] Genna S, Trovalusci F, Tagliaferri V. Indentation test to study the moisture absorption effect on CFRP composite. *Compos Part B* 2017; 124: 1–8.

[14] Cysne Barbosa AP, P. Fulco AP, S.S. Guerra E, et al. Accelerated aging effects on carbon fiber/epoxy composites. *Compos Part B Eng* 2017; 110: 298–306.

[15] Saeed MU, Chen Z, Chen Z, et al. Compression behavior of laminated composites subjected to damage induced by low velocity impact and drilling. *Compos Part B Eng* 2014; 56: 815–820.

[16] Cauich-Cupul JI, Pérez-Pacheco E, Valadez-González A, et al. Effect of moisture absorption on the micromechanical behavior of carbon fiber/epoxy matrix composites. *J Mater Sci* 2011; 46: 6664–6672.

[17] Attukur Nandagopal R, Gin Boay C, Narasimalu S. An empirical model to predict the strength degradation of the hygrothermal aged CFRP material. *Compos Struct* 2020; 236: 111876.

[18] Behera A, Vishwakarma A, Thawre MM, et al. Effect of hygrothermal aging on static behavior of quasi-isotropic CFRP composite laminate. *Compos Commun* 2020; 17: 51–55.

[19] Cheng X, Baig Y, Li Z. Effects of hygrothermal environmental conditions on compressive strength of CFRP stitched laminates. *J Reinf Plast Compos* 2011; 30:

110–122.

[20] Hunkley JA, Connell JW. Resin Systems and Chemistry: Degradation Mechanisms and Durability. In: Pochiraju K V, Tandon G, Schoeppner GA (eds) *Long-Term Durability of Polymeric Matrix Composites*. 2012.

[21] Grammatikos SA, Evernden M, Mitchels J, et al. On the response to hygrothermal aging of pultruded FRPs used in the civil engineering sector. *Mater Des* 2016; 96: 283–295.

[22] Gautier L, Mortaigne B, Bellenger V. Interface damage study of hydrothermally aged glass-fibre-reinforced polyester composites. *Compos Sci Technol* 1999; 59: 2329–2337.

[23] Korkees F, Alston S, Arnold C. Directional diffusion of moisture into unidirectional carbon fiber/epoxy Composites: Experiments and modeling. *Polym Compos* 2018; 39: E2305–E2315.

[24] Grammatikos SA, Zafari B, Evernden MC, et al. Moisture uptake characteristics of a pultruded fibre reinforced polymer flat sheet subjected to hot/wet aging. *Polym Degrad Stab* 2015; 121: 407–419.

[25] Vasiliev V V, Morozov E V. *Advanced Mechanics of Composite Materials*. 2nd ed. Oxford: Elsevier, 2007.

[26] Ray BC. Temperature effect during humid ageing on interfaces of glass and carbon fibers reinforced epoxy composites. *J Colloid Interface Sci* 2006; 298: 111–117.

[27] Dao B, Hodgkin J, Krstina J, et al. Accelerated aging versus realistic aging in aerospace composite materials. V. The effects of hot/wet aging in a structural epoxy composite. *J Appl Polym Sci* 2010; 115: 901–910.

[28] Meng M, Rizvi MJ, Le HR, et al. Multi-scale modelling of moisture diffusion coupled with stress distribution in CFRP laminated composites. *Compos Struct* 2016; 138: 295–304.

[29] Almudaihesh F, Holford K, Pullin R, et al. The influence of water absorption on unidirectional and 2D woven CFRP composites and their mechanical performance. *Compos Part B Eng* 2020; 182: 107626.

[30] Stannett V. Simple Gases. In: Crank J, Park GS (eds) *Diffusion in Polymers*. New York: Academic Press, 1968, pp. 41–73.

[31] Arnold JC, Alston SM, Korkees F. An assessment of methods to determine the directional moisture diffusion coefficients of composite materials. *Compos Part A Appl Sci Manuf* 2013; 55: 120–128.

[32] Karbhari VM, Xian G. Hygrothermal effects on high VF pultruded unidirectional carbon/epoxy composites: Moisture uptake. *Compos Part B Eng* 2009; 40: 41–49.

[33] Hübner M, Lepke D, Hardi E, et al. Online Monitoring of Moisture Diffusion in Carbon Fiber Composites Using Miniaturized Flexible Material Integrated Sensors. *Sensors* 2019; 19: 1748.

[34] Pan Y, Xian G, Li H. Numerical modeling of moisture diffusion in an

unidirectional fiber-reinforced polymer composite. *Polym Compos* 2019; 40: 401–413.

[35] Huo Z, Anandan S, Xu M, et al. Investigation of three-dimensional moisture diffusion modeling and mechanical degradation of carbon/bismaleimide composites under seawater conditioning. *J Compos Mater* 2018; 52: 1339–1351.

[36] Surathi P, Karbhari VM. *Hygrothermal Effects on Durability and Moisture Kinetics of Fiber-reinforced Polymer Composites*. San Diego, https://rosap.ntl.bts.gov/view/dot/27688 (2006).

[37] Wong TC, Broutman LJ. Water in epoxy resins Part II. Diffusion mechanism. *Polym Eng Sci* 1985; 25: 529–534.

[38] Carter HG, Kibler KG. Langmuir-Type Model for Anomalous Moisture Diffusion In Composite Resins. *J Compos Mater* 1978; 12: 118–131.

[39] Crank J. *The Mathematics of Diffusion*. Second. Clarendon Press, 1975.

[40] Shen C-H, S. Springer G. Moisture Absorption and Desorption of Composite Materials. *J Compos Mater* 1976; 10: 2–20.

[41] Rao RMVGK, Balasubramanian N, Chanda M. Factors Affecting Moisture Absorption in Polymer Composites Part I: Influence of Internal Factors. *J Reinf Plast Compos* 1984; 3: 232–245.

[42] Rao RMVGK, Chanda M, Balasubramanian N. Factors Affecting Moisture Absorption in Polymer Composites Part II: Influence of External Factors. *J Reinf Plast Compos* 1984; 3: 246–253.

[43] ASTM International. D5229/D5229M-14e1 Standard Test Method for Moisture Absorption Properties and Equilibrium Conditioning of Polymer Matrix Composite Materials. West Conshohocken, PA: ASTM International, 2014. Epub ahead of print 2014. DOI: https://doi.org/10.1520/D5229_D5229M-14E01.

[44] Hexcel. HexPly Prepreg. 2013; 35.

[45] Bank L, Gentry TR, Barkatt A. Accelerated Test Methods to Determine the Long-Term Behavior of FRP Composite Structures: Environmental Effects. *J Reinf Plast Compos* 1995; 14: 559–587.

[46] ASTM International. Standard Test Method for Glass Transition Temperature (DMA Tg) of Polymer Matrix Composites by Dynamic Mechanical Analysis (DMA). West Conshohocken, PA: ASTM International, 2015. Epub ahead of print 2015. DOI: https://doi.org/10.1520/D7028-07R15.

[47] Maxwell AS, Broughton WR, Dean G, et al. *Review of Accelerated Ageing Methods and Lifetime Prediction Techniques for Polymeric Materials*. 2005.

[48] Korkees F, Arnold C, Alston S. An investigation of the long-term water uptake behavior and mechanisms of carbon fiber/977-2 epoxy composites. *Polym Eng Sci* 2018; 58: 2175–2184.

[49] Choi HS, Ahn KJ, Nam J, et al. Hygroscopic aspects of epoxy / carbon fiber composite laminates in aircraft environments. *Compos Part A Appl Sci Manuf* 2001; 32: 709–720.

[50] Karmaker AC. Effect of water absorption on dimensional stability and impact

energy of jute fibre reinforced polypropylene. *J Mater Sci Lett* 1997; 16: 462–464.

[51] Espert A, Vilaplana F, Karlsson S. Comparison of water absorption in natural cellulosic fibres from wood and one-year crops in polypropylene composites and its influence on their mechanical properties. *Compos Part A Appl Sci Manuf* 2004; 35: 1267–1276.

[52] Wang Z, Xian G, Zhao X-L. Effects of hydrothermal aging on carbon fibre/epoxy composites with different interfacial bonding strength. *Constr Build Mater* 2018; 161: 634–648.